

Mask-adaptive Gated Convolution and Bi-directional Progressive Fusion Network for Depth Completion

Tingxuan Huang¹, Jiacheng Miao¹, Shizhuo Deng^{1,2}, Tong Jia^{1,3}, Dongyue Chen^{1,2,3,*}

¹ College of Information Science and Engineering,

Northeastern University Shenyang 110819, Liaoning, China

² National Frontiers Science Center for Industrial Intelligence and Systems Optimization,
Northeastern University, Shenyang 110819, Liaoning, China

³ Foshan Graduate School of Innovation,
Northeastern University, Foshan 528311, Guangdong, China

Abstract

Depth completion is a critical task for handling depth images with missing pixels, which can negatively impact further applications. Recent approaches have utilized Convolutional Neural Networks (CNNs) to reconstruct depth images with the assistance of color images. However, vanilla convolution has non-negligible drawbacks in handling missing pixels. To solve this problem, we propose a new model for depth completion based on an encoder-decoder structure. Our model introduces two key components: the Mask-adaptive Gated Convolution (MagaConv) architecture and the Bi-directional Progressive Fusion (BP-Fusion) module. The MagaConv architecture is designed to acquire precise depth features by modulating convolution operations with iteratively updated masks, while the BP-Fusion module progressively integrates depth and color features, utilizing consecutive bi-directional fusion structures in a global perspective. Extensive experiments on popular benchmarks, including NYU-Depth V2, DIML, and SUN RGB-D, demonstrate the superiority of our model over state-of-the-art methods. We achieved remarkable performance in completing depth maps and outperformed existing approaches in terms of accuracy and reliability.

1. Introduction

Depth completion, also known as depth inpainting, is widely used in applications such as 3D reconstruction [1], virtual reality [19], and autonomous vehicles [16]. It aims to replace missing pixels in raw depth maps captured by sensors with reliable ones. Commonly used sensors for acquiring depth maps include Time-of-flight, structured light, Lidar, binocular vision, etc. However, due to inherent sensor limitations, factors such as sensor noise, reflections, ab-

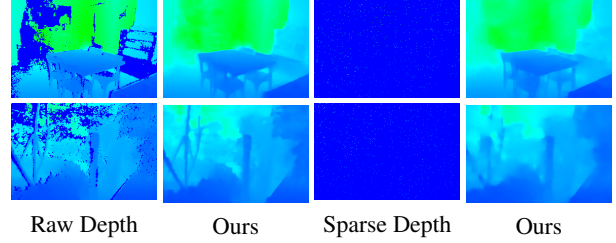


Figure 1. Showcases of raw depth and sparse depth maps with invalid data in the benchmark datasets DIML, and the corresponding depth completion results of our proposed model. The first column presents the depth completion tasks from indoor scenarios, while the second column displays outdoor circumstances.

sorption, or sharp boundaries can inevitably result in missing information in the depth map. Addressing these challenges and developing robust depth completion algorithms is essential for obtaining more accurate and complete depth maps from the raw depth data.

Recently, convolutional neural networks (CNNs) have gained significant popularity for depth completion tasks. Many approaches have utilized convolutional encoder-decoder architectures, such as U-Net and its variants [22], to capture multi-scale contextual information and generate depth predictions. However, these approaches face limitations due to the vanilla convolution operation, which treats all pixels equally, including the missing ones in the raw depth map. This can lead to feature deviations and error propagation to neighboring regions. To address these limitations, researchers have proposed various approaches, such as dilated convolutions [33], partial convolutions [13], gated convolutions [34], and attention-guided gated convolutions [2]. These convolutional methods aim to mitigate the negative impact of missing pixels and improve accuracy by repositioning kernels or suppressing unreliable features. How-

ever, most of these approaches have not fully exploited the potential benefits of the valid pixel distribution in extracting precise depth features. To tackle this issue, we introduce a novel convolution operation modulated by iteratively updated masks called Mask-adaptive Gated Convolution (MagaConv) to enhance depth feature extraction.

To further improve the accuracy of depth completion, researchers have explored the integration of color information. RGB-guided approaches commonly involve the fusion of color and depth features by concatenating them and employing vanilla convolution operations, such as CSPN and its variant [4, 5, 17]. However, these approaches have inherent limitations. Firstly, they neglect the differences between color and depth modalities: depth features primarily capture geometric properties, while RGB features convey surface appearance and texture. Simply concatenating these features may not fully exploit their complementary information. Secondly, the fusion process in these approaches is typically performed by convolution operations, which are localized and may not effectively capture the global perspective required for comprehensive fusion. To address these challenges, we propose a novel bi-directional progressive fusion module called BP-Fusion, to consider their distinct characteristics and facilitate thorough fusion of two modalities.

In general, our main contribution can be summarized as follows:

- We develop a convolutional encoder-decoder network that utilizes our newly proposed MagaConv and BP-Fusion to generate high-quality completion of the depth image.
- A Mask-adaptive Gated Convolution (MagaConv) is proposed to extract reliable depth features, which utilizes iteratively updated masks to modulate the convolution operation.
- A Bi-directional Progressive Fusion module (BP-Fusion) is proposed, based on consecutive bi-directional fusion modules in a global perspective, aiming to thoroughly fuse color and depth features.
- Experimental results demonstrate that our model outperforms the state-of-the-art on three popular benchmarks, including NYU-Depth V2, DIML, and SUN RGB-D datasets.

2. Related Works

2.1. Depth Completion

The task of depth completion aims to generate dense depth maps from incomplete depth images. Ma and Qu, et al. [18, 21] employed a basic encoder-decoder network to obtain dense depth maps. S2DNet and Deepdnet [9, 10] proposed a two-stage network, in which the initial stage focuses on acquiring approximate depth images, and the sub-

sequent stage is to enhance the primary results. Gu, Liu, and Zhu, et al. [8, 14, 39] introduced a residual depth map completion network, which utilizes a residual map to enhance the initial completion image, resulting in sharper edges. SPN, CSPN, CSPN++, and NLSPN [3, 5, 15, 20] optimized the SPN algorithms to enhance the prediction of unfamiliar depth values by effectively incorporating known depth information. However, the predicted depth maps still exhibit blurriness attributed to the limitations of vanilla convolution operations in encoding depth features.

2.2. Feature Extraction

The presence of missing or unreliable depth pixels in the raw depth map poses a challenge when using vanilla convolutions to extract features. This is because vanilla convolutions treat all pixels equally, including those with missing or unreliable depth values. To overcome artifacts caused by vanilla convolutions, researchers have proposed a series of convolutions [6, 13, 30, 34] to avoid the impact of missing value. Liu et al. [13] proposed Partial convolution, which utilizes a mask to distinguish between valid and invalid pixels. The convolution operation is exclusively applied to the valid pixels, and the mask is iteratively updated according to the convolution results. Yu et al. [34] introduced a Gated Convolution that generalizes partial convolution by providing a learnable dynamic feature selection mechanism. Lu et al. [6] proposed Fast Fourier Convolution (FFC), which has a larger receptive field and a cross-scale fusion within the convolution unit. Xie et al. [30] introduced a Learnable Bidirectional Attention Maps (LBAM) module that learns feature re-normalization and mask-updating in an end-to-end manner. Nevertheless, these methods did not adequately exploit the use of masks. To tackle this issue, we propose the MagaConv architecture, a new convolution operation that is modulated by iteratively updated masks. This approach is designed to enhance the accuracy and reliability of depth feature extraction.

2.3. Multi-modal Data Fusion

Multi-modal feature fusion is another essential aspect compared to depth feature extraction. Xu and Imran [11, 31] used direct channel-wise concatenation to fuse features. Zhong, Li, Zhou, et al. [12, 37, 38] designed adaptive modules to realize global feature fusion throughout the encoding and decoding procedures. Chen et al. [2] proposed Attention Guided Gated-Convolution (AG-GConv) to fuse depth and color features at different scales, effectively reducing the negative impacts of invalid depth data on the reconstruction. Additionally, Rignet, GuideNet, and Ssgp [23, 28, 32] proposed a dual-modal encoder-decoder network that uses the reconstructed color features to guide the depth encoding process, enabling a multi-level fusion within the network architecture. In this paper, We propose the Bi-directional Pro-

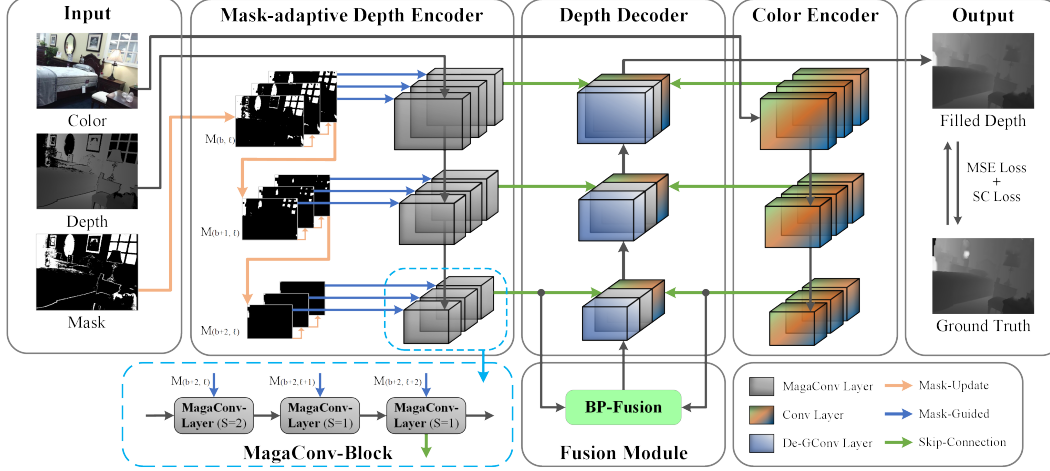


Figure 2. Pipeline of our depth completion model, including the MagaConv architecture, the BP-Fusion module we proposed, and the De-GConv Layer proposed by [2]. $M_{(b,l)}$ represents adaptive masks, where b and l represent the block and layer, respectively.

gressive Fusion (BP-Fusion) module, which aims to comprehensively fuse color and depth cues from a global perspective.

3. Methods

In this section, we present our overall depth completion network architecture and its two key components: Mask-adaptive Gated Convolution (MagaConv) and Bi-directional Progressive Fusion (BP-Fusion). Additionally, we introduce the overall loss function, including an MSE loss and a Structure-Consistency loss.

3.1. Overall Network Architecture

The pipeline of our model is shown in Fig. 2, it aims to fill all the missing depth pixels in the raw depth images. The network consists of four components: (i) Mask-adaptive Depth Encoder, (ii) Color Encoder, (iii) Fusion Module, and (iv) Depth Decoder.

(i) The Mask-adaptive Depth Encoder is designed to extract reliable depth features while effectively handling the impact of missing values. The feature extraction procedure operates in four levels: Mask-adaptive depth encoder, MagaConv-Blocks, MagaConv-Layers, and MagaConv operation. The Mask-adaptive depth encoder takes raw depth images and their corresponding masks as inputs, and outputs the precise depth feature with the guidance of adaptive masks. It consists of three MagaConv-Blocks, each of which downsamples the depth feature by half. Within each block, the input passes through three consecutive MagaConv-Layers. The first layer has a stride of 2, while the subsequent ones have a stride of 1. Only the output features from the last layer of each block are then forwarded to the decoder through skip connections. The

MagaConv-Layer is guided by different masks, which are updated at every block and layer. Furthermore, the details of the MagaConv-Layer and MagaConv operation will be introduced in the sec. 3.2.

(ii) The Color Encoder takes RGB images as inputs and transforms them into essential depth-relevant features. It follows a similar structure to the depth encoder branch, except for the substitution of MagaConv Layers. Instead, the Color Encoder utilizes three vanilla convolutional layers at each block, accompanied by residual connections and without pre-trained parameters.

(iii) The Fusion Module efficiently fuses features of the high-level depth and color features. It employs the proposed BP-Fusion architecture, in which the fusion process operates in a progressive manner, to capture complementary information from both modalities, leading to an improved quality of the depth completion results. The detailed structure of the BP-Fusion will be illustrated in the sec. 3.3.

(iv) The Depth Decoder reconstructs the complete depth image using a multi-scale skip-connected decoder. This decoder is adapted from the Gated De-convolution module proposed by [2]. By incorporating the skip connections from multiple scales, the Depth Decoder is able to generate high-quality depth completion results.

3.2. Mask-adaptive Gated Convolution

The presence of missing or unreliable pixels of the image poses a challenge when using vanilla convolutions to extract features, which treat all pixels equally. To solve this problem, Partial Convolution [13] and Gated Convolution [34] extracted the features with the help of masks, avoiding negative impact from the missing values. However, it neglects the suitability of the pixels within their corresponding receptive fields. As a result, we propose the MagaConv

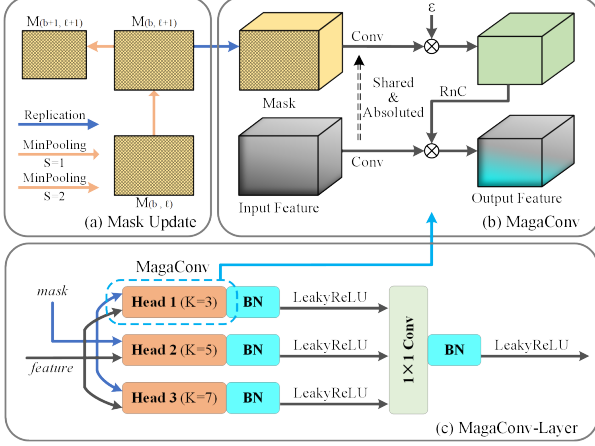


Figure 3. Details of the MagaConv and MagaConv-Layer operation, which utilizes masks to modulate the convolution process and extract more reliable depth features.

MagaConv Operation. Considering a raw depth map $D \in \mathbb{R}^{h \times w}$ and a vanilla convolution kernel ω with the size of $k \times k$ that processes a group of pixels. The output $O^{Conv}_{(i,j)}$ at the position (i, j) can be defined as follows:

$$O^{Conv}_{(i,j)} = \sum_{x=-k}^k \sum_{y=-k}^k \omega_{(i+x,j+y)} * D_{(i+x,j+y)} \quad (1)$$

Then, denote $M \in \mathbb{R}^{h \times w}$ as the corresponding mask of the D , in which 1 of the mask map represents a missing depth pixel. It can be defined as follows:

$$M_{i,j} = \begin{cases} 1 & \text{if } D_{i,j} \leq 0 \\ 0 & \text{if } D_{i,j} > 0 \end{cases} \quad (2)$$

This mask can be used to measure the suitability of the pixels within the receptive fields of ω . Specifically, we suppose that the larger absolute parameter in ω is likely to be an important reference. If the missing value is related to that parameter, the output of the convolutional kernel becomes less reliable at that position. Based on the observation, we adopt the same convolution kernel with absolute parameters $|\omega|$ to conduct convolution operation with the mask M , quantitatively measuring the suitability in a specific position. This operation is defined as follows:

$$O^{Mask}_{i,j} = \epsilon * \sum_{x=-k}^k \sum_{y=-k}^k |\omega_{(i+x,j+y)}| * M_{(i+x,j+y)} \quad (3)$$

where $O^{Mask}_{i,j}$ indicates the unsuitability of a convolution kernel when it encounters inaccurate areas at the position (i, j) , and $\epsilon \in (0, 1)$ is a learnable parameter used to normalize $O^{Mask}_{i,j}$, enhancing the training robustness. Notably, the mask M is replicated along the channel axis before the

convolution operation, ensuring that its shape remains the same with the depth features. The value $O^{Mask}_{i,j}$ can be transformed into a penalty term, effectively punishing convolutional kernels that heavily rely on invalid areas. The penalty term is defined as follows:

$$O^{MaG}_{i,j} = RnC(O^{Mask}_{i,j}) \otimes O^{Conv}_{i,j} \quad (4)$$

where \otimes denotes element-wise multiplication, and the RnC (Reverse-and-Cut) is an activation function we proposed, which is defined as follows:

$$RnC(x) = [ReLU(e^{-x} - 0.5)] \times 2, x > 0 \quad (5)$$

It is evident that $RnC(x) \in [0, 1]$. Similar to the ReLU activation function, RnC also incorporates a non-linear and threshold-based activation function during the guiding process, enabling convolution kernels to learn intricate relationships. In this situation, the output of RnC serves to evaluate the suitability of the convolution kernel in a specific area. It can also be regarded as a gating signal that modulates the convolution output O^{Conv} .

MagaConv-Layer. The MagaConv operation is utilized within the MagaConv-Layer, following the specific architecture described in sec. 3.1 (i). In each layer, three parallel MagaConv operations are executed in separate heads to acquire multi-scale features, as shown in Fig. 3 (c). Specifically, each MagaConv head takes the same depth features and binary mask as inputs and utilizes a different kernel size to obtain multi-scale features. These features are then fused together using a vanilla convolution with a kernel size of 1×1 . Importantly, the parallel-head architecture does not significantly increase the overall computational consumption, since the total number of channels remains the same compared to a single-head structure. Therefore, this structure can be easily implemented in any framework as part of the forward pass.

Mask Update. To provide particular instructions for each MagaConv-Layer at different scales, the masks are updated in every block and layer based on different rules, as shown in Fig. 3 (a). In the layer l of the block b , the mask update rule can be defined as follows:

$$\begin{aligned} M(b, l+1) &= MinPooling2D(M(b, l), s=1) \\ M(b+1, l) &= MinPooling2D(M(b, l+2), s=2) \end{aligned} \quad (6)$$

where s denotes the stride parameter. To ensure the size of the mask matches that of the depth feature, s is aligned with the stride of the MagaConv-Layer. In this manner, a specific mask pixel is updated to be valid if surrounding areas contain at least one valid mark, and gradually the mask will become fully valid.

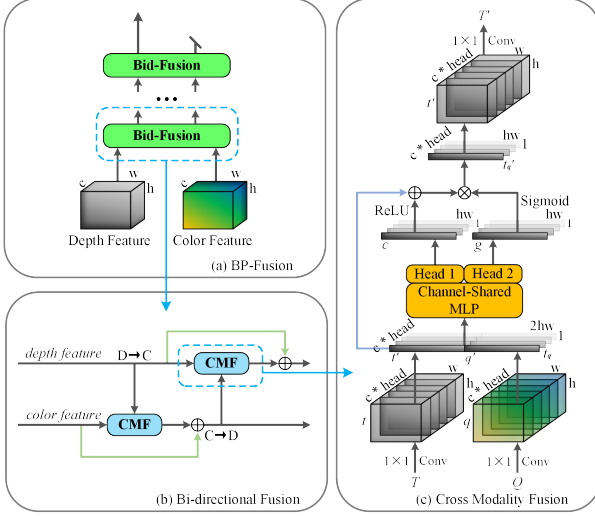


Figure 4. Details of Bi-directional Fusion Module.

Motivation Analysis. The MagaConv architecture extracts precise depth features from three key aspects. (i) The MagaConv operation suppresses unreliable features by modulating the convolutional process. It quantitatively evaluates the suitability between pixels and the convolution kernels using the masks, which differentiate valid and invalid pixels. The measurements are transformed into a gating signal through the RnC activation function, enabling the modulation of the convolutional output. As a result, more reliable depth features can be extracted from incomplete depth maps. (ii) The integration of MagaConv-Block, MagaConv-Layer, and parallel-head structures enables the extraction of multi-scale depth features with more reliable feature representation, thus enhancing the reconstruction quality. (iii) The MagaConv architecture incorporates iteratively updated masks, which are updated in every MagaConv-Block and MagaConv-Layer according to specific rules. These masks provide precise instructions for the multi-scale architectures, further enhancing the accuracy and effectiveness of the depth completion model.

3.3. Bi-directional Progressive Fusion (BP-Fusion)

As mentioned in the related work, the incorporation of a fusion module is essential for combining color features with depth features. This integration is required to carefully select relevant color features that can enrich the depth feature and consequently lead to an improved reconstruction performance. Therefore, we propose a new module named BP-Fusion that thoroughly fuses features from two modalities in a progressive manner.

The architecture of the BP-Fusion module consists of a sequence of Bid-Fusion modules, as depicted in Fig. 4 (a), which ensures a gradual and thorough fusion from differ-

ent modalities. The specific structure of each Bid-Fusion [block], illustrated in Fig. 4 (b), consists of two parallel streams for depth and color features, respectively. The information exchange of the two streams occurs in two directions. Firstly, the depth features are introduced via the forward pass to modulate the color feature ($D \rightarrow C$). secondly, the [reconstructed] color features are transmitted through the backward pass to enhance the representation of depth features ($C \rightarrow D$).

At each intersection of the two passes, a Cross-Modal Fusion (CMF) module is proposed to conduct the fusion of color and depth process from a global perspective, as shown in Fig. 4 (c). The CMF module takes features from the two modalities as input, denoted as the target feature $T \in \mathbb{R}^{h \times w \times c}$ and the query feature $Q \in \mathbb{R}^{h \times w \times c}$ as input. It selectively fuses the information from the query feature and outputs only the target feature. Specifically, the module operates as follows: Firstly, T and Q are expanded along the channel axis through 1×1 convolution and split into $c * head$ slices, resulting in slices $t \in \mathbb{R}^{h \times w \times 1}$ and $q \in \mathbb{R}^{h \times w \times 1}$. The value of $head$ is typically set to 3. Secondly, each slice t and q is reshaped to $hw \times 1$ and denoted as t' and q' , and concatenated together to form combined embeddings $t_q \in \mathbb{R}^{hw \times 2}$. These combined embeddings are then passed through channel-shared MLP structure, which consists of two hidden layers with a fixed number of ReLU neurons, and two output heads that generate correction signals $c \in \mathbb{R}^{hw \times 1}$ and gating signals $g \in \mathbb{R}^{hw \times 1}$, respectively. The overall transformation process can be defined as follows:

$$t'_q = ReLU(c + t') \otimes Sigmoid(g) \quad (7)$$

where \otimes denotes element-wise multiplication, t' is the residual connection of the target vectors. At last, the output embedded is reshaped to the original size, concatenated, and fused along the channel axis to obtain the final output of the CMF module, denoted as $T' \in \mathbb{R}^{h \times w \times c}$.

Motivation Analysis. In general, the BP-Fusion module achieves thorough fusion because of three key advantages. (i) The BP-Fusion module iteratively refines the depth features, allowing for fusing more informative features, and leading to improved performance in subsequent tasks. (ii) The Bid-Fusion achieves efficient fusion by a bi-directional feature transformation. The forward pass ($D \rightarrow C$) allows for filtering and transforming color features into depth-relevant expressions, while the backward pass ($C \rightarrow D$) effectively enriches the depth features using the beneficial color features, thereby ensuring a comprehensive mixture of features from both modalities. (iii) The CMF module facilitates global perspective fusion utilizing a Channel-Shared MLP structure, significantly enhancing the reliability of the fused features. Specifically, the neurons inside the MLP store numerous fixed patterns of cross-modal alignment,

which can be processed by computing the similarity between all input pixels and each parameter. In this way, hidden cues between color and depth features are transformed into a high-order view at the hidden layer, and produced a correction signal c and a gating signal g by two output heads. These signals are designed to conduct precise spatial adjustments for the target feature representation, improving the overall quality. Furthermore, the Channel-Shared structure mitigates excessive parameters and overfitting, thus enhancing overall network robustness and accelerating both training and inference speeds.

3.4. Loss

The loss functions used in depth completion tasks are designed to minimize overall differences or areas with significant deficiencies in the predicted depth maps. The Mean Average Error (MAE) and Mean Squared Error (MSE) are commonly used loss functions in this context. However, it is worth noting that depth maps often contain crucial boundary information that may not be effectively captured by these standard losses. Therefore, we employed Structure-Consistence (SC) loss function to address the limitation.

The Structure-Consistence loss function can be formulated as follows:

$$\mathcal{L}_{sc} = \frac{1}{N} \sum_{i=1}^N \left| \nabla D_{pred}^{(i)} - \nabla D_{gt}^{(i)} \right|_2^2 \quad (8)$$

\mathcal{L}_{sc} represents the structure-consistence loss, N is the number of samples in the training process, $D_{pred}^{(i)}$ is the predicted depth map for the i -th sample, $D_{gt}^{(i)}$ is the corresponding ground truth depth map, ∇ denotes the Laplacian operator for extracting edge information, and $|\cdot|_2^2$ denotes the squared Euclidean norm.

During the training process of our model, in addition to utilizing \mathcal{L}_{sc} , the MSE loss function is also employed, marked as \mathcal{L}_{mse} . The overall loss function is given by:

$$\mathcal{L}_{all} = \mathcal{L}_{mse} + \mathcal{L}_{sc} \quad (9)$$

By incorporating the SC loss alongside the MSE loss, the model is encouraged to minimize not only the pixel-wise depth errors but also to preserve the structural integrity and edge information in the predicted depth maps. This leads to more visually accurate and detailed depth completion results.

4. Experiments

4.1. Experimental Setup

We conducted comprehensive experiments on three popular benchmark datasets: NYU-Depth V2, DIML, and SUN RGB-D to validate the performance of the model.

NYU-Depth V2 [26] is the most authoritative and widely used benchmark datasets for depth image completion, which contains 408,473 images collected in 464 different indoor scenes, and 1449 officially labeled images for evaluation.

DIML [7] is a recently introduced datasets of 2 million images captured in diverse indoor and outdoor settings. This datasets includes images with typical edge shadows and irregular holes, providing a robust evaluation benchmark for assessing the adaptability of our model to various invalid patterns. We utilize 2000 pairs of labeled samples from the indoor part of the datasets according to the official split.

SUN RGB-D [27] is an extensive datasets comprising 10,335 densely captured RGB-D images obtained from four different sensors. The datasets covers 19 primary scene categories, providing a diverse range of scenes for evaluation. In accordance with the default protocol, we partitioned the datasets into 4,845 images for training and 4,659 ones for testing.

Metrics. The evaluation of indoor depth completion results is based on three criteria: Root Mean Squared Error (RMSE), Relative Error (Rel), and Threshold Accuracy (δ_t) with thresholds $t = 1.10, 1.25, 1.25^2, 1.25^3$.

Implementation Details. Our model was implemented using the PyTorch framework and trained on an NVIDIA RTX 3090 GPU for a total of 80 epochs. We adopted the SGD optimizer for training, with a momentum term of 0.95 and a weight decay term of 10^{-4} . The initial learning rate was set to 1×10^{-3} and was halved during the plateau period. The model was trained using end-to-end training methodology.

4.2. Ablation Studies

To optimize the proposed framework and evaluate its performance, a series of ablation experiments were carried out on the NYU-Depth V2 datasets. At first, we constructed a baseline model (scheme A) similar to our proposed model, which retained the fundamental architecture of the encoder-decoder network but utilized vanilla convolution instead of MagaConv operation and employed direct concatenation of depth and color features at the bottom neck instead of the BP-Fusion module. Based on this baseline, we formed three categories with eight different protocols (schemes B to I) by combining various solutions for each module. Schemes B-D were designed to evaluate the effectiveness of MagaConv, schemes E-G aimed to validate the influence of the BP-Fusion module, and schemes H and I were used to assess different loss functions. The details of different protocols are shown in Tab. 1.

(i) On MagaConv. In the first group of experiments, we investigated the impact of different convolution operations on the depth encoder while maintaining the remaining

Scheme	MagaConv	Parallel-Head	Partial-Conv	BP-Fusion	Bi-direction	CMF	Conv	\mathcal{L}_{mse}	\mathcal{L}_{sc}	RMSE↓	Rel↓	$\delta_{1.10}$ ↑
A	-	-	-	-	-	-	-	✓	✓	0.188	0.028	95.6
B	✓	✓	-	-	-	-	-	✓	✓	0.109	0.015	97.3
C	✓	-	-	-	-	-	-	✓	✓	0.114	0.016	97.0
D	-	✓	✓	-	-	-	-	✓	✓	0.134	0.018	96.4
E	-	-	-	✓	✓	✓	-	✓	✓	0.128	0.017	96.7
F	-	-	-	✓	-	✓	-	✓	✓	0.148	0.020	95.9
G	-	-	-	✓	✓	-	✓	✓	✓	0.143	0.018	96.2
H	✓	✓	-	✓	✓	✓	-	✓	-	0.091	0.013	98.1
I	✓	✓	-	✓	✓	✓	-	✓	✓	0.085	0.011	98.5

Table 1. Ablation study results for different schemes of the pipeline on the NYU-Depth V2 datasets. The model is set to take the raw depth maps as inputs ($\mathcal{R} \rightarrow \mathcal{G}$).

settings identical to the baseline. Scheme B incorporated the complete settings of our proposed MagaConv module, which demonstrated improved performance compared to the baseline (0.109 vs. 0.188 in RMSE). This suggests that the MagaConv module effectively filters out invalid features, resulting in a more reliable feature representation. In scheme C, we made a modification by removing the multiple parallel heads from each MagaConv Layer and instead used a single head with a 5×5 kernel. This led to a slight decline in performance across all metrics (0.114 RMSE vs. 0.109 in RMSE). This indicates that the parallel-head structure plays a crucial role in capturing multi-scale features, which are important for effectively completing depth images. In scheme D, we replaced the MagaConv with the Partial-Conv [13], and observed a deterioration in performance across all metrics (0.134 vs. 0.109 in RMSE). This suggests that the gated signal generated by adaptive masks indeed enhances the reliability of the depth features.

(ii) On BP-Fusion. In the second group, various fusion schemes were integrated into the baseline. Scheme E, which implements our proposed BP-Fusion module, demonstrated a significant improvement in performance compared to scheme A (0.128 vs. 0.188 in RMSE). This indicates that the fusion of depth and color features within the BP-Fusion module leads to a more accurate reconstruction of depth maps. In scheme F, we replaced the bi-directional fusion with a unidirectional approach by cutting off the forward pass from depth to color, resulting in performance deterioration (0.148 vs. 0.128 in RMSE). This suggests that the forward pass benefits the filtering and learning of color features, which, in turn, strengthens the depth feature through the backward pass from color to depth. In scheme G, we replaced the CMF module with a vanilla convolution applied to the concatenation of the two modalities. This resulted in a noticeable decrease in all metrics (0.143 vs. 0.128 in RMSE), indicating that the global modulation provided by the CMF module plays an important role in the comprehensive integration of depth and color features.

(iii) On loss function. In the last group, two different settings of loss functions are evaluated. Scheme I,

which integrated both the MSE loss \mathcal{L}_{mse} and the structure-consistency loss \mathcal{L}_{sc} , significantly outperforms scheme H that only employed the MSE loss (0.085 vs. 0.091 in RMSE). Notably, scheme I exhibited an approximately 15% improvement in the Rel metric (0.013 vs. 0.011). It demonstrates the effectiveness of integrating the structure-consistency loss into our approach, leading to enhanced performance in depth map completion.

In conclusion, the scheme I integrates all of our proposed modules with the baseline model and achieves the highest scores on all three metrics. This outcome serves as strong evidence for the effectiveness of our proposed modules in improving accuracy.

4.3. Comparison to State-of-the-art

To evaluate the performance of our proposed model, we conducted comparative experiments against state-of-the-art depth completion methods [2, 4, 17, 20, 24, 29, 35]. Our model used the best settings identified in the ablation study and carried out experiments under two different tasks. The first task ($\mathcal{R} \rightarrow \mathcal{G}$) requires the model to inpaint the raw depth images, aligning with the application requirements of Time-of-Flight (TOF) depth cameras. The second task ($\mathcal{G}^* \rightarrow \mathcal{G}$) demands the model to reconstruct a depth image from a sparsely selected set of 500 depth pixels, more in line with the application requirements of LiDAR.

On NYU-Depth V2. The quantitative comparison results with other state-of-the-art methods [2, 4, 17, 20, 32, 35, 36] on NYU-Depth V2 datasets are shown in Tab. 2. Our model achieves the best results in terms of all three metrics across both the two tasks. It surpasses the RMSE of the second-best method by approximately 5% (0.085 vs. 0.091) in the first task and 15% (0.077 vs. 0.090) in the second task. The visualized results of several typical scenes in the NYU-Depth V2 datasets are shown in Fig. 5. Our model exhibits the most reliable and highest-quality reconstruction results. Specifically, in the first two rows, there are severe missing areas in the window region. The results of all the other competing methods show obvious artifacts in these regions, while our results demonstrate more vivid and

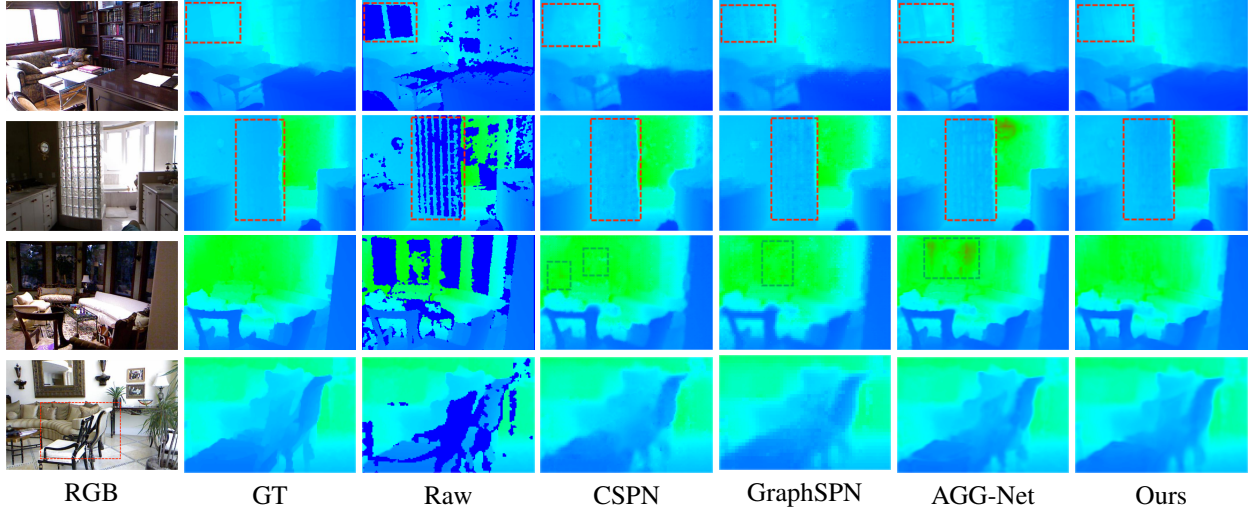


Figure 5. Depth completion comparison results with different methods on NYU-Depth V2 of the setting $\mathcal{R} \rightarrow \mathcal{G}$.

Setting	Method	RMSE↓	Rel↓	$\delta_{1.25} \uparrow$	$\delta_{1.25^2} \uparrow$	$\delta_{1.25^3} \uparrow$
$\mathcal{R} \rightarrow \mathcal{G}$	CSPN [4]	0.173	0.02	96.3	98.6	99.5
	NLSPN [20]	0.153	0.015	98.6	99.6	99.9
	RDF-GAN [29]	0.139	0.013	98.7	99.6	99.9
	GraphSPN [17]	0.133	0.012	98.8	99.7	99.9
	AGG-Net [2]	0.092	0.014	99.4	99.9	100.0
	CFormer [35]	0.091	0.012	99.6	99.9	100.0
	Ours	0.085	0.011	99.6	99.9	100.0
$\mathcal{G}^* \rightarrow \mathcal{G}$	CSPN [4]	0.117	0.016	99.2	99.9	100.0
	ACMNet [36]	0.105	0.015	99.4	99.9	100.0
	NLSPN [20]	0.092	0.012	99.6	99.9	100.0
	RDF-GAN [29]	0.103	0.012	99.4	99.9	100.0
	RigNet [32]	0.096	0.013	99.6	99.9	100.0
	AGG-Net [2]	0.096	0.012	99.5	99.9	100.0
	GraphSPN [17]	0.090	0.012	99.6	99.9	100.0
	CFormer [35]	0.090	0.012	99.6	99.9	100.0
	Ours	0.077	0.011	99.7	100.0	100.0

Table 2. Quantitative comparison results with competing methods on NYU-Depth V2 datasets. \mathcal{R} denotes the raw depth maps, \mathcal{G}^* denotes the sparse depth pixels sampled from the ground truth \mathcal{G} .

Benchmark	Method	RMSE↓	Rel↓	$\delta_{1.25} \uparrow$	$\delta_{1.25^2} \uparrow$	$\delta_{1.25^3} \uparrow$
DIML	CSPN [4]	0.162	0.033	96.1	98.7	99.6
	DfuseNet [25]	0.143	0.023	98.4	99.4	99.9
	DM-LRN [24]	0.149	0.015	99.0	99.6	99.9
	AGG-Net [2]	0.078	0.011	99.6	99.9	100.0
	Ours	0.062	0.011	99.8	99.9	100.0
SUN	CSPN [4]	0.295	0.137	95.6	97.5	98.4
	NLSPN [20]	0.267	0.063	97.3	98.1	98.5
	RDF-GAN [29]	0.255	0.059	96.9	98.4	99.0
	AGG-Net [2]	0.202	0.038	98.5	99.0	99.4
	Ours	0.206	0.038	98.2	99.1	99.6

Table 3. Quantitative comparison results with other methods on DIML, and SUN RGB-D datasets of the setting $\mathcal{R} \rightarrow \mathcal{G}$.

precise details. In the third row, the ground-truth depth map of the five windows should be dense and uniform, whereas

other methods exhibit unrealistic artifacts. Additionally, in the bottom row, our results show sharper edges of the chair, indicating that our approach outperforms other methods at finer scales.

On DIML and SUN RGB-D. Regarding the dataset DIML, as shown in Tab. 3 (a), our model is also compared to state-of-the-art methods [2, 4, 24, 25]. Our model outperforms these competing methods in all three metrics, with a remarkable 20% improvement in RMSE. For the datasets SUN RGB-D, as shown in Tab. 3 (b), our model is evaluated against comparative methods including [2, 4, 20, 29], and also achieved competing performance. Compared to the AGG-Net [2], although our method may not exhibit a significant advantage in terms of the three metrics, it is worth noting that our model has only 30% of the parameter count compared to the AGG-Net (169M vs. 48M). This reduction in parameters leads to significantly improved training and inference speeds.

All the above experimental results provide strong evidence that our method provides an advanced and effective approach to depth completion. The proposed model surpasses existing works on three widely used benchmark datasets, showcasing its superior performance across diverse scenarios.

5. Conclusion

In conclusion, we proposed a novel model for depth completion, which introduces the MagaConv and the BP-Fusion to enhance accuracy and reliability. The MagaConv architecture modulates the convolution process guided by iteratively updated masks, facilitating precise depth feature extraction. The BP-Fusion module progressively integrates depth and color features using consecutive Bid-Fusion structures, ensuring reliable fusion from a

global perspective. Through extensive experiments on popular datasets, including NYU-Depth V2, DIML, and SUN RGB-D, we demonstrated the superiority of our model over existing state-of-the-art methods. Overall, our proposed method offers an effective solution for applications that rely on accurate and reliable depth information. We believe our model could make significant contributions to further tasks including image inpainting, multi-modal image segmentation, 3D reconstruction, etc.

References

- [1] Benedicte Bascle and Rachid Deriche. Stereo matching, reconstruction and refinement of 3d curves using deformable contours. In *ICCV*, 1993. 1
- [2] Dongyue Chen, Tingxuan Huang, Zhimin Song, Shizhuo Deng, and Tong Jia. Agg-net: Attention guided gated-convolutional network for depth image completion. *arXiv preprint arXiv:2309.01624*, 2023. 1, 2, 3, 7, 8
- [3] Xinjing Cheng, Peng Wang, and Ruigang Yang. Depth estimation via affinity learned with convolutional spatial propagation network. In *Proceedings of the European conference on computer vision (ECCV)*, pages 103–119, 2018. 2
- [4] Xinjing Cheng, Peng Wang, and Ruigang Yang. Learning depth with convolutional spatial propagation network. *TPAMI*, 2019. 2, 7, 8
- [5] Xinjing Cheng, Peng Wang, Chenye Guan, and Ruigang Yang. Cspn++: Learning context and resource aware convolutional spatial propagation networks for depth completion. In *Proceedings of the AAAI Conference on Artificial Intelligence*, pages 10615–10622, 2020. 2
- [6] Lu Chi, Borui Jiang, and Yadong Mu. Fast fourier convolution. *Advances in Neural Information Processing Systems*, 33:4479–4488, 2020. 2
- [7] Jaehoon Cho, Dongbo Min, Youngjung Kim, and Kwanghoon Sohn. A large RGB-D dataset for semi-supervised monocular depth estimation. *CoRR*, 2019. 6
- [8] Jiaqi Gu, Zhiyu Xiang, Yuwen Ye, and Lingxuan Wang. Denselidar: A real-time pseudo dense depth guided depth completion network. *IEEE Robotics and Automation Letters*, 6(2):1808–1815, 2021. 2
- [9] Praful Hambarde and Subrahmanyam Murala. S2dnet: Depth estimation from single image and sparse samples. *IEEE Transactions on Computational Imaging*, 6:806–817, 2020. 2
- [10] Girish Hegde, Tushar Pharale, Soumya Jahagirdar, Vaishakh Nargund, Ramesh Ashok Tabib, Uma Mudanagudi, Basavaraja Vandrotti, and Ankit Dhiman. Deepdnet: Deep dense network for depth completion task. In *Proceedings of the IEEE/CVF Conference on Computer Vision and Pattern Recognition*, pages 2190–2199, 2021. 2
- [11] Saif Imran, Yunfei Long, Xiaoming Liu, and Daniel Morris. Depth coefficients for depth completion. In *2019 IEEE/CVF Conference on Computer Vision and Pattern Recognition (CVPR)*, pages 12438–12447. IEEE, 2019. 2
- [12] Ang Li, Zejian Yuan, Yonggen Ling, Wanchao Chi, Chong Zhang, et al. A multi-scale guided cascade hourglass network for depth completion. In *Proceedings of the IEEE/CVF Winter Conference on Applications of Computer Vision*, pages 32–40, 2020. 2
- [13] Guilin Liu, Fitsum A Reda, Kevin J Shih, Ting-Chun Wang, Andrew Tao, and Bryan Catanzaro. Image inpainting for irregular holes using partial convolutions. In *ECCV*, 2018. 1, 2, 3, 7
- [14] Lina Liu, Xibin Song, Xiaoyang Lyu, Junwei Diao, Mengmeng Wang, Yong Liu, and Liangjun Zhang. Fcfr-net: Feature fusion based coarse-to-fine residual learning for depth completion. In *AAAI*, 2021. 2
- [15] Sifei Liu, Shalini De Mello, Jinwei Gu, Guangyu Zhong, Ming-Hsuan Yang, and Jan Kautz. Learning affinity via spatial propagation networks. *Advances in Neural Information Processing Systems*, 30, 2017. 2
- [16] Shaoshan Liu, Liangkai Liu, Jie Tang, Bo Yu, Yifan Wang, and Weisong Shi. Edge computing for autonomous driving: Opportunities and challenges. *Proceedings of the IEEE*, 2019. 1
- [17] Xin Liu, Xiaofei Shao, Bo Wang, Yali Li, and Shengjin Wang. Graphcspn: Geometry-aware depth completion via dynamic gcns. In *European Conference on Computer Vision*, pages 90–107. Springer, 2022. 2, 7, 8
- [18] Fangchang Ma and Sertac Karaman. Sparse-to-dense: Depth prediction from sparse depth samples and a single image. In *2018 IEEE international conference on robotics and automation (ICRA)*, 2018. 2
- [19] Richard A Newcombe, Shahram Izadi, Otmar Hilliges, David Molyneaux, David Kim, Andrew J Davison, Pushmeet Kohi, Jamie Shotton, Steve Hodges, and Andrew Fitzgibbon. Kinectfusion: Real-time dense surface mapping and tracking. In *IEEE international symposium on mixed and augmented reality*, 2011. 1
- [20] Jinsun Park, Kyungdon Joo, Zhe Hu, Chi-Kuei Liu, and In So Kweon. Non-local spatial propagation network for depth completion. In *Computer Vision–ECCV 2020: 16th European Conference, Glasgow, UK, August 23–28, 2020, Proceedings, Part XIII 16*, pages 120–136. Springer, 2020. 2, 7, 8
- [21] Chao Qu, Ty Nguyen, and Camillo Taylor. Depth completion via deep basis fitting. In *Proceedings of the IEEE/CVF Winter Conference on Applications of Computer Vision*, pages 71–80, 2020. 2
- [22] Olaf Ronneberger, Philipp Fischer, and Thomas Brox. U-net: Convolutional networks for biomedical image segmentation. In *Medical Image Computing and Computer-Assisted Intervention (MICCAI)*, 2015. 1
- [23] René Schuster, Oliver Wasenmuller, Christian Unger, and Didier Stricker. Ssgp: Sparse spatial guided propagation for robust and generic interpolation. In *Proceedings of the IEEE/CVF Winter Conference on Applications of Computer Vision*, pages 197–206, 2021. 2
- [24] Dmitry Senushkin, Mikhail Romanov, Ilia Belikov, Nikolay Patakin, and Anton Konushin. Decoder modulation for indoor depth completion. In *2021 IEEE/RSJ International*

- Conference on Intelligent Robots and Systems (IROS)*, pages 2181–2188. IEEE, 2021. 7, 8
- [25] Shreyas S Shivakumar, Ty Nguyen, Ian D Miller, Steven W Chen, Vijay Kumar, and Camillo J Taylor. DfuseNet: Deep fusion of rgb and sparse depth information for image guided dense depth completion. In *2019 IEEE Intelligent Transportation Systems Conference (ITSC)*, 2019. 8
- [26] Nathan Silberman, Derek Hoiem, Pushmeet Kohli, and Rob Fergus. Indoor segmentation and support inference from rgbd images. In *Computer Vision – ECCV 2012*, pages 746–760, 2012. 6
- [27] Shuran Song, Samuel P. Lichtenberg, and Jianxiong Xiao. Sun rgb-d: A rgb-d scene understanding benchmark suite. In *Proceedings of the IEEE Conference on Computer Vision and Pattern Recognition (CVPR)*, 2015. 6
- [28] Jie Tang, Fei-Peng Tian, Wei Feng, Jian Li, and Ping Tan. Learning guided convolutional network for depth completion. *IEEE Transactions on Image Processing*, 30:1116–1129, 2020. 2
- [29] Haowen Wang, Mingyuan Wang, Zhengping Che, Zhiyuan Xu, Xiuquan Qiao, Mengshi Qi, Feifei Feng, and Jian Tang. Rgb-depth fusion gan for indoor depth completion. In *Proceedings of the IEEE/CVF Conference on Computer Vision and Pattern Recognition*, pages 6209–6218, 2022. 7, 8
- [30] Chaohao Xie, Shaohui Liu, Chao Li, Ming-Ming Cheng, Wangmeng Zuo, Xiao Liu, Shilei Wen, and Errui Ding. Image inpainting with learnable bidirectional attention maps. In *Proceedings of the IEEE/CVF international conference on computer vision*, pages 8858–8867, 2019. 2
- [31] Yan Xu, Xinge Zhu, Jianping Shi, Guofeng Zhang, Hujun Bao, and Hongsheng Li. Depth completion from sparse lidar data with depth-normal constraints. In *Proceedings of the IEEE/CVF International Conference on Computer Vision*, pages 2811–2820, 2019. 2
- [32] Zhiqiang Yan, Kun Wang, Xiang Li, Zhenyu Zhang, Jun Li, and Jian Yang. Rignet: Repetitive image guided network for depth completion. In *European Conference on Computer Vision*, pages 214–230. Springer, 2022. 2, 7, 8
- [33] Fisher Yu and Vladlen Koltun. Multi-scale context aggregation by dilated convolutions. *arXiv preprint arXiv:1511.07122*, 2015. 1
- [34] Jiahui Yu, Zhe Lin, Jimei Yang, Xiaohui Shen, Xin Lu, and Thomas S Huang. Free-form image inpainting with gated convolution. In *CVPR*, 2019. 1, 2, 3
- [35] Youmin Zhang, Xianda Guo, Matteo Poggi, Zheng Zhu, Guan Huang, and Stefano Mattoccia. Completionformer: Depth completion with convolutions and vision transformers. In *Proceedings of the IEEE/CVF Conference on Computer Vision and Pattern Recognition*, pages 18527–18536, 2023. 7, 8
- [36] Shanshan Zhao, Mingming Gong, Huan Fu, and Dacheng Tao. Adaptive context-aware multi-modal network for depth completion. *IEEE Transactions on Image Processing*, 2021. 7, 8
- [37] Yiqi Zhong, Cho-Ying Wu, Suyu You, and Ulrich Neumann. Deep rgb-d canonical correlation analysis for sparse depth completion. *Advances in Neural Information Processing Systems*, 2019. 2
- [38] Zhengming Zhou and Qiulei Dong. Self-distilled feature aggregation for self-supervised monocular depth estimation. In *ECCV*, 2022. 2
- [39] Yufan Zhu, Weisheng Dong, Leida Li, Jinjian Wu, Xin Li, and Guangming Shi. Robust depth completion with uncertainty-driven loss functions. In *Proceedings of the AAAI Conference on Artificial Intelligence*, pages 3626–3634, 2022. 2